CrossMark

On Correlating Elastic Properties of the Porous Structure to Pore Attributes

Siddhartha Patra[1] · **Abhijit Chanda**[1]

Abstract The correlation between the stiffness and porosity of the porous material is studied for many decades. In most cases the goal was to propose an equation correlating the fractional change in elastic modulus to the net porosity for a given pore geometry (often spherical). The mechanical behavior of the porous material is often assumed to be isotropic with few exceptions where the directionality is addressed. In the current study through numerical analysis in Ansys APDL it is shown that the variation of elastic modulus with net porosity is also affected by the factors like shape, size, slenderness and relative orientation of the pores. In addition a general equation is proposed to represent the effect of net porosity and aspect ratio on the variation of Young's moduli in different directions. The behavior of the porous structure is found to be neither isotropic nor completely anisotropic. If the solid phase is isotropic, then the behavior of the porous structure is best classified as orthotropic.

Keywords Porosity · Pore shape · Pore size · Pore orientation · Elasticity · Orthotropy · Isotropy · Additive manufacturing · Ansys · APDL · Finite element

Introduction

Presence of a minor extent of porosity is inevitable in engineering components, developed through conventional manufacturing processes. However, it is when the cumulative pore volume becomes a significant fraction of the total volume of the specimen; the porous material starts behaving differently and can no longer be treated as a continuum. Therefore, studying engineering behavior of porous materials is becoming increasingly important particularly since porosity is not just the manufacturing flaw but sometimes it is considered to be a desirable feature as well. Porous materials find their application in many fields of engineering given their ability to provide desired level of permeability (membrane like structures) or

✉ Siddhartha Patra
siddharthapatra16@gmail.com

1 Department of Mechanical Engineering, Jadavpur University, Kolkata 700032, India

🍪 Springer

in-growth of biological tissues (biomedical implants) etc. Numerous studies have been conducted on porous materials mostly from the latter half of the last century to this date. Most of these works focus on establishing a key relationship between the stiffness of the porous material (E) and the stiffness of its *solid phase* (E_0), often comparing the porous structure to a composite with two phases—the solid material and the empty space. Some of these works are theoretical; many of them are semi-empirical and empirical in nature yet the bottom-line remains that the simplest rule of mixture $E = E_0(1 - p)$ is an over simplification where the net porosity p is the ratio of the pore volume to the total volume of the specimen. Even a linear relationship such as Dewey's [1] model:

$$E = E_0(1 - bp), \qquad (1)$$

where b is a material parameter, has found limited applicability. The nonlinearity of the relationship between the stiffness of the porous structure and the porosity is well appreciated. The basic nature of the Nonlinear empirical relationships proposed by Duckworth [2] and Spriggs [3] is given below,

$$E = E_0 \exp(-bp), \qquad (2)$$

where b is a material parameter. One may replace Young's modulus from the above expression with the bulk or shear modulus [2,3]. This type of relationships were effective but lacked theoretical support since at $p = 1$ or zero solid phase, the stiffness of the structure would not become zero. Wang [4] through theoretical derivation for periodically arranged spherical polyhedrons presented a nonlinear relationship between stiffness and porosity. The nonlinear relationship required numerical solution. Wang showed that for smaller values of porosity ($p \geq 0.20$), one may approximate such relationship to the one presented by Spriggs or Duckworth. For higher values of porosity, the exponential fit would involve a polynomial of the p value, i.e.,

$$E = E_0 \exp(c_1 p + c_2 p^2 + \cdots) \qquad (3)$$

Phani and Niyogi [5] proposed a power law fit as follows:

$$E = E_0(1 - ap)^b, \qquad (4)$$

where $a = \frac{1}{p_{cr}}$ and b are material parameters. In the above expression, p_{cr} represents the critical value of the porosity at which the stiffness of the material becomes zero.

Ramakrishnan and Arunachalam [6] used assembly of hollow spherical solid geometries to model porous structure. Their theoretical work yields:

$$M = M_0(1 - p)^2/(1 + bp) \qquad (5)$$

as the common expression for all elastic moduli, i.e., Young's modulus, shear and bulk modulus.

Adachi and Sakka [7] presented a comparative study of different porosity models by fitting them to the experimental results of porous silica heated between 700 and 1050 °C. Choren et al. [8] provided a comprehensive review on these relations of general form $E = E_0 f(p)$. Whether empirical or theoretical, one thing common about all these expressions is the assumed isotropy of the porous structures.

To define a linear elastic material model even with isotropy, one would need atleast two material parameters from the set $[E, K, G, \nu]$, i.e., Young's modulus, bulk modulus, shear modulus and Poisson's ratio. Since (E, ν) make a convenient pair of material parameters in past few decades the variation of Poisson's ratio with porosity has also been studied by researchers. If the bulk and the shear moduli are supposed to have the same variation as the
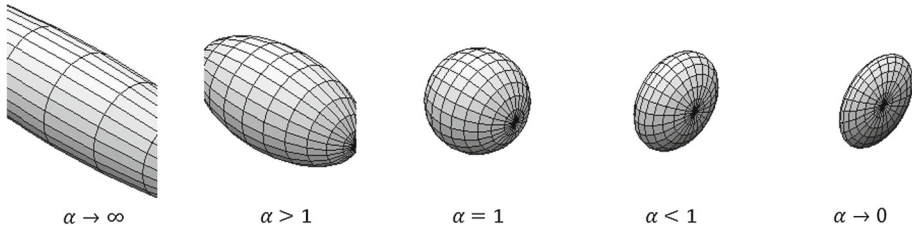
$\alpha \to \infty$　　　$\alpha > 1$　　　$\alpha = 1$　　　$\alpha < 1$　　　$\alpha \to 0$

Fig. 1 Variety of spheroidal pores

Young's modulus, $\nu(= \nu_0)$ becomes a constant. That however, is not true as it seems from various studies. Dunn and Ledbetter [9] presented a self-consistent theoretical analysis on spheroidal pores of a variety of aspect ratio (α). The expressions of effective Poisson's ratios for different aspect ratios (Fig. 1) as functions of porosity are given below.

When $\alpha \to \infty$, the pore shape can be categorized as needle like. The effective Poisson's ratio is given by:

$$\nu_{eff} = \frac{-15\nu_0 + p(8\nu_0 - 5)(\nu_0 + 1)}{-15 + 4p(4\nu_0 - 5)(\nu_0 + 1)}. \tag{6}$$

For spherical pores ($\alpha = 1$), the expression for effective Poisson's ratio is given by:

$$\nu_{eff} = \frac{2\nu_0(5\nu_0 - 7) + p(5\nu_0 - 3)(\nu_0 + 1)}{2(5\nu_0 - 7) + p(15\nu_0 - 13)(\nu_0 + 1)}. \tag{7}$$

Ramakrishnan and Arunachalam [6] presented the following expression for effective Poisson's ratio,

$$\nu_{eff} = \frac{1}{4} \frac{4\nu_0 + 3p - 7p\nu_0}{1 + 2p - 3p\nu_0} \tag{8}$$

Nielsen [10] presents a universal expression for the variation of different moduli with porosity, i.e.,

$$\frac{E_{eff}}{E_0} = \frac{K_{eff}}{K_0} = \frac{G_{eff}}{G_0} = \frac{(1-p)^2}{\left[1 + \left(\frac{1}{\rho} - 1\right)p\right]} \tag{9}$$

where ρ is a shape factor which characterizes the pore geometry for low porosity (discrete pores). The equality in the above expression simply indicates little or no variation of Poisson's ratio. Ashkin et al. [11] obtained best fit to their experimental data with $\rho = 0.4$. Thus,

$$\frac{E_{eff}}{E_0} = \frac{(1-p)^2}{[1 + 1.5p]} \tag{10}$$

Phani and Sanyal [12] fitted Nielsen's equation to the experimental results of Adachi and Sakka [7] on the variation of bulk modulus with porosity. The best fit was obtained for $\rho = 0.476$. Thus,

$$\frac{K_{eff}}{K_0} = \frac{(1-p)^2}{[1 + 1.1p]} \tag{11}$$

Using above two expressions and also using the relationship between bulk modulus and Young's modulus for isotropic materials, i.e., $K = \frac{E}{3(1-2\nu)}$, following expression for effective Poisson's ratio is obtained:

$$\nu_{eff} = 0.5 - \frac{(1 + 1.1p)(1 - 2\nu_0)}{2(1 + 1.5\nu_0)} \tag{12}$$

Nielsen [13] extended his work to viscoelastic materials to study the variation of elasticity and damping with porosity.

Phani and Sanyal [14] presented a study on the interdependence of the variation of the different moduli (bulk, shear, Young's) for isotropic ceramic materials based on the theory of Mori–Tanaka [15]. Phani and Sanyal [14] proposed the following expression for the shear modulus.

$$G = G_0 \left[\frac{2}{3} (1 + \nu_0) \left(\frac{E}{E_0} \right) + \frac{1 - 2\nu_0}{3} \left(\frac{E}{E_0} \right)^n \right], \tag{13}$$

where n is a material parameter and the quantities with suffix 0 represent the properties of the solid phase.

Finite element analysis has also been conducted on porous geometries. Meguid et al. [16] and Girogi et al. [17] used periodically arranged shell type elements to model metallic foams. While Meguid et al. showed an agreement of the FE solutions with the experimental results, Girogi et al discussed the variation of stress-strain behavior with density of the foam. Badiche et al. [18] and Kaoua et al. [19] used periodically arranged Timoshenko beam elements to model metallic foams. Badiche et al. shows an agreement of simulation and experimental results in two different directions (rolling and transverse). Kaoua et al. on the other hand discusses the variation of anisotropy and Young's modulus with the change of the geometry of the cross section of the beam. The last two articles showed non-isotropic behavior of the porous structures. However, they did not discuss how the mechanical properties of the porous structure may change with the change in the periodic arrangements of the beams or shells because of the change in pore structure, orientation or net porosity.

The theoretical and empirical relations discussed above give nonlinear relationships between the stiffness of the porous structure and the net pore volume. However, the parameters involved in the relation are material dependent. Thus, the parameters have to be calibrated for each material and also no single formula is valid for all porous materials. For instance Kovacik [20] uses the expression (Eq. 4) proposed by Phani and Niyogi [5] to establish the correlation between stiffness and pore volume for three different materials. As per their study, the value of critical porosity p_c, at which stiffness goes to zero, ranges from 0.31 to 0.53 for different base materials and compositions and the value of f changes from 0.94 to 1.66.

Porosity remains the only independent variable in all such relations. However, there is more to the pores than the net porosity, such as, pore size, pore shape and their distribution. If the pores of different shapes sizes and aspect ratios are arranged randomly in a porous material, the behavior of the material is expected to be isotropic. However, the material starts showing directionality, i.e., orthotropicity, when pores of a given aspect ratio align in a given direction. Examples of alignment of pores can be found in nature as well as man-made objects. Figure 2a shows the porous structures in mushrooms [21,22]. The image on the left shows hexagonal pores, and the image on the right shows elliptical pores. In either case, the pores are wider in radial direction than the tangential direction. Also in both the cases each pore is surrounded by six neighboring pores, a configuration later illustrated in Fig. 5a, b. Artificial honeycombs [23] shown in Fig. 2c have the similar stacking of hexagonal pores. Porous structure of cacellous bones [24] shown in Fig. 2b has irregularly shaped pores, yet they follow a typical pattern of alignment. The pores seem to be wider in the vertical direction and narrower in the horizontal.

Figure 2d depicts a nanocomposite scaffold for bone tissue engineering [25]. This contains systematically arranged rectangular pores. Additive manufacturing techniques such as EBM [26] can be used to manufacture orthopedic implants such as the knee implant shown in Fig. 2e. Such structures are created by fusing a stack of layers which often consist of pores, in
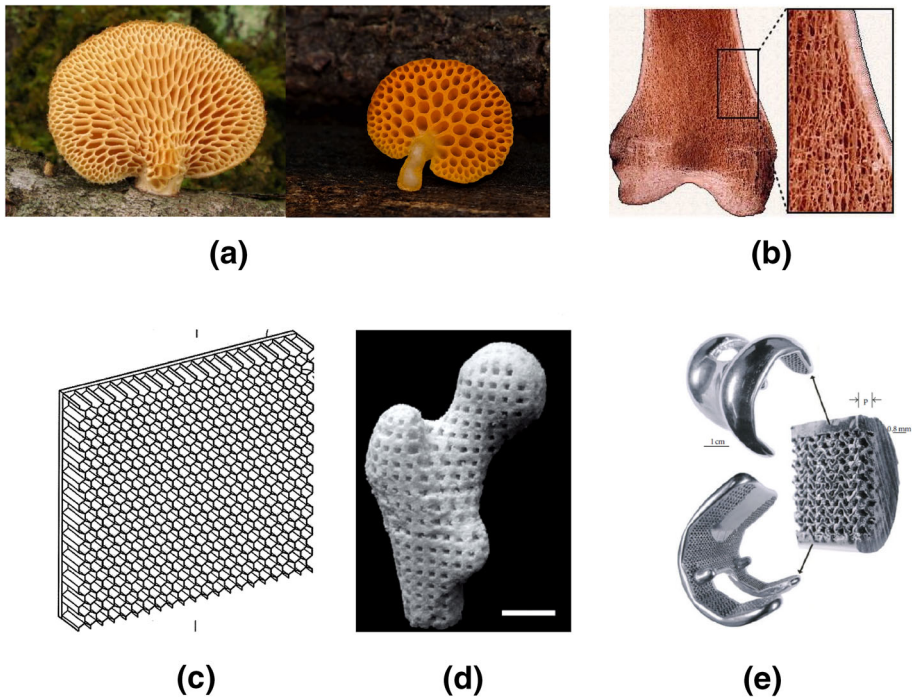
Fig. 2 Natural and artificial porous structures with systematically arranged pores. **a** Mushroom porous structures. **b** Porous structure of cacellous bone. **c** Artificial honeycomb. **d** Nanocomposite Scaffold. **e** Porous knee implant

order to reduce weight, that follow a systematic arrangement. While standard test practices exist for the bulk component, testing procedure for the structural properties of individual layers are not readily available. In this article numerical technique is used to determine the mechanical properties of a planar structure with pores, thereby developing an understanding of the variation of structural properties with pore attributes. Such an understanding would be contextual in the current era of 3-D printing and additive manufacturing. Many of these structures are porous with a wide variation in pore architecture. The current study could be helpful in the assessment of the mechanical behavior of such structure so as to help design modifications prior to manufacturing. Here finite element analysis is conducted on planar porous structures with variation of porosity, pore geometry (shape and aspect ratio), pore size and pore orientation. In future, it is envisaged that, this work may be extended into 3-D porous structures.

Finite Element Procedure

Finite element analyses were conducted on 2-D porous structures using ANSYS APDL (Ansys Parametric Design Language). The choice of the classic APDL environment over the more advanced Workbench environment is motivated by the availability of better control over pore geometry, mesh, choice of element, etc. Another advantage of using the classic environment is to be able to use an APDL script in the batch mode multiple times, with minor modifications in the script for the pore shape, pore size, net pore volume etc.

Description of the Porous Structures

The *solid model* consists of uniformly distributed pores in a thin square planar geometry of area 1 mm^2. The size of thestructure serves as a reference to evaluate the relative pore size.

The pore geometries are taken to be circle, ellipse, hexagon and rectangle. The aspect ratio for elliptical pores is defined by the ratio of the minor axis to major axis ($\alpha = b/a$). The aspect ratio for hexagonal and rectangular pores is defined as the aspect ratio of the inscribed ellipse. Moreover, it is rather helpful to use a parametric angle β with which the points on the ellipse can be defined (taking the centre of the ellipse as the origin) as:

$$x = a \cos \beta \ \& \ y = b \sin \beta. \tag{14}$$

The physical angle ϕ is thus defined as:

$$\tan \phi = \alpha \tan \beta. \tag{15}$$

An ellipse can not be directly created in ANSYS. Instead two B-spline curves were fitted through the twelve key points for $\beta = (i - 1)\frac{\pi}{6} + \frac{\pi}{2} \forall i \in [1, 2, \ldots, 12]$, defining the boundary of the ellipse. The B-spline curves were then used to create the bounded area (Fig. 3).

The vertices of a rectangular pore are defined as ($\pm a, \pm b$). For the hexagonal pore, the vertices are given by the coordinates:

$$x_i = \bar{a} \cos \beta_i; \quad y_i = \bar{b} \sin \beta_i, \tag{16}$$

where $\beta_i = \frac{\pi}{6} + \frac{(i-1)\pi}{3} \forall i \in [1, 2, \ldots, 6]$ also, $\bar{a} = \frac{2}{\sqrt{3}}a; \bar{b} = \alpha\bar{a}$ (Fig. 4).

The pores are considered to be evenly distributed such that if the porosity is increased gradually to the maximum value ($p_{max} = \frac{\frac{\pi}{2}}{\sqrt{3}} \approx 0.90$ for circular or elliptical pores and
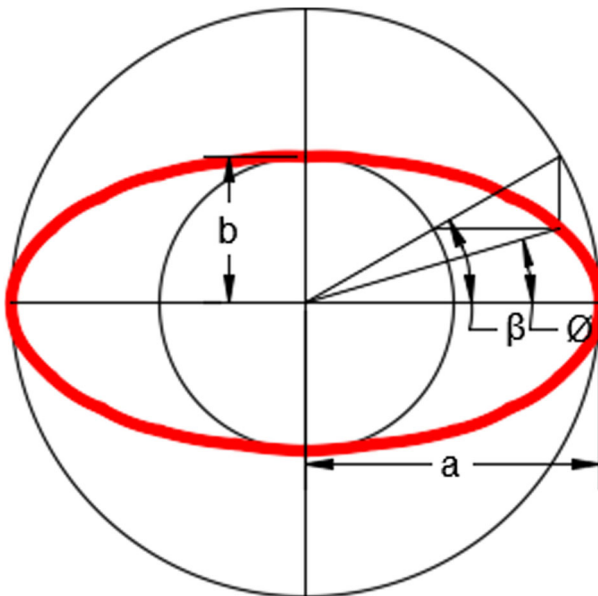

Fig. 3 The parametric and physical angles of an ellipse

Fig. 4 Equivalence of aspect ratios of different pore geometries
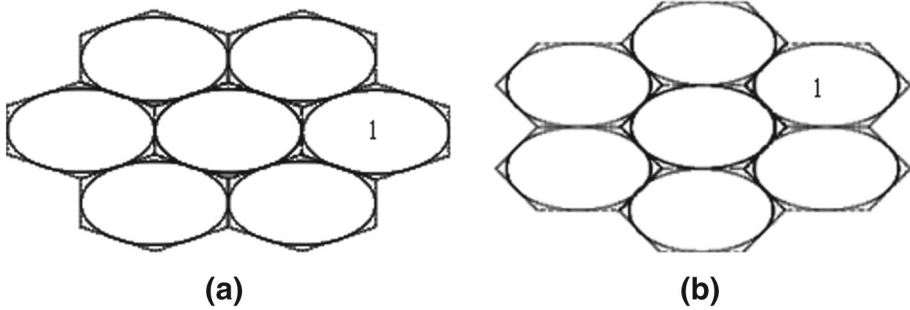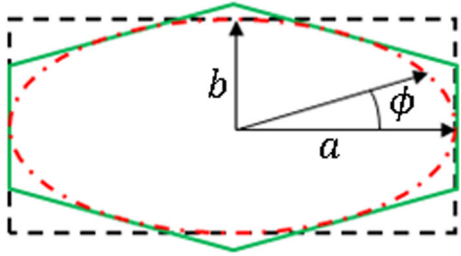

Fig. 5 Relative orientation of pores. **a** Configuration 1. **b** Configuration 2

1.00 for hexagonal or rectangular pores), the pores touch each other. The closed packing happens by surrounding each pore with six others, thus, each neighboring pore spanning $\Delta\beta = 60° = \frac{\pi}{3}$ of parametric angle. The common tangents form a hexagon.

The two configurations shown in Fig. 5 have the same porosity ($p = p_{\max}$) but in the first diagram the contact happens along the major axes and in the second along the minor axes. The two configurations are identical for circular pores. However, for the elliptical pores, keeping the porosity constant, an infinite number of such configurations can be imagined with the first neighboring ellipse (marked as 1 in Fig. 5) making the contact at an initial angle $\beta_0 \in \left(0, \frac{\pi}{6}\right)$, with the major axis of the central ellipse. Thus, the above configurations represent two extreme scenarios. Turns out, in addition to bulk porosity, shape, aspect ratio and size, such configurations affect the mechanical properties. Here only the Configuration 1 is considered. The Configuration 2 can be effectively modeled by making the aspect ratio $\alpha > 1$. The equivalence between Configuration 1 and 2 is given by the following relations

$$\left\{ \begin{array}{l} E_{xx}^2\,(p, \alpha) := E_{yy}^1\left(p, \frac{1}{\alpha}\right) \\ E_{yy}^2\,(p, \alpha) := E_{xx}^1\left(p, \frac{1}{\alpha}\right) \end{array} \right\}, \tag{17}$$

where the superscripts represent the configuration number.

Geometry and Meshing

A pore with its surrounding hexagon represents a unit cell (except for a rectangle, where the unit cell is rectangular). The unit cell repeats itself about all the six sides several times to finally cover the entire geometry. For the ease of meshing the size of the geometry is approximated to a semi-integral $\left(\frac{n}{2}, \text{where } n \in I\right)$ multiple of the sides of the bounding box of the hexagon.
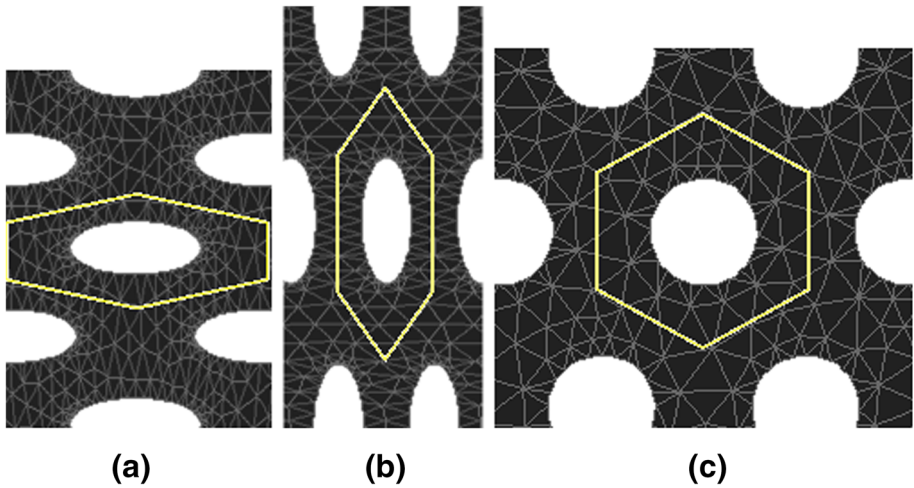
Fig. 6 FE mesh with 25% porosity. **a** $\alpha < 1$. **b** $\alpha > 1$. **c** $\alpha = 1$

When p is less than the maximum value, the sides of the hexagon are simply bigger by a factor $\sqrt{\frac{p_{max}}{p}}$ (Fig. 6).

A 2-D analysis is performed with plane stress settings. Plane stress model is the idealization of a thin structure under planar loads with no constraints along the direction of thickness.

ANSYS provides a wide variety over the choice of elements for plane stress analysis. A geometry which has been made complex by the presence of several pores, is bound to generate triangular element. If the default choice remains either the PLANE182 linear Quad elements or PLANE183 serendipity quadratic Quad elements, degenerate triangles would be produced as a substantial fraction of the total mesh count. Thus, PLANE183 elements with six node triangle shape (Keyopt (1) = 1) were chosen. Six node triangle elements are free from volumetric or shear locking, hourglass modes and they are not serendipity elements and also have curved sides. Smart sizing feature is used for mesh refinement based on pore size and curvature. Mesh refinement was performed upto the point of convergence of the results of the solution.

A linear elastic isotropic material model was assigned to the entire geometry. This material model requires two parameters namely the Young's modulus (E_0) and Poisson's ratio ($\nu = 0.3$). At the interior of the geometry at any point E_0 would represent the local stiffness of the material but for the entire geometry with many pores, the global stiffness is expected to be quite low.

Solution with Different Load Cases and Post-processing

For faster meshing and solution, a quarter symmetric model (symmetric about x axis as well as y axis) is used. This reduces the DOF count to $\frac{1}{4}$th (Fig. 7).

A displacement controlled analysis is performed to determine the stiffness for the porous structure. Displacement boundary conditions are applied at the extreme right end and the extreme top end. The model was loaded in both x and y axes, with x axis being parallel to the major axis of the elliptical pores and y axis to the minor axis. The steps of analysis are given below.
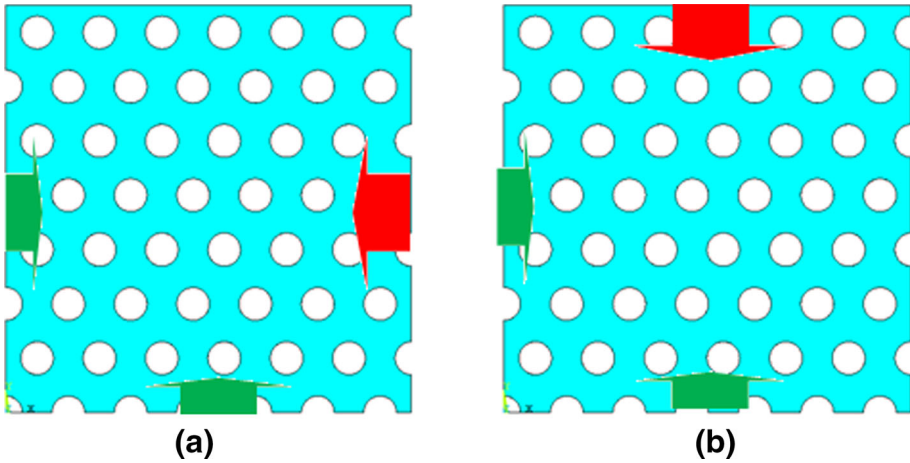
Fig. 7 Loading conditions. **a** Load case 1: Parallel to major axis. **b** Load case 2: Parallel to minor axis. *Note*: Green arrows represent the symmetry boundary conditions and red arrows represent the compressive load

(1) Load case 1:

    (a) At first the extreme top end is left free and a uniform compressive displacement is applied to the extreme right. With the interest of focusing only in the linear elastic behavior of the component a compressive strain of $|\epsilon_c| = \delta = 0.003$ was applied.

    (b) Effective stiffness (E_{xx}^{eff}) and the lateral deflection behavior (ν_{xy}^{eff}) are noted down. To determine the Young's modulus, all nodes on the y axis are selected and the nodal forces are summed up. The total force is divided the span of the component in y axis. Since the model represents unit thickness (Keyopt(3) = 0), this value represents E_{xx}^{eff}.

To determine the value of the Poisson's ratio, all the nodes at the top end are selected and their average deflection in the y direction (u_y) is divided by the applied compression $(u_x = -\delta \times (x_{max} - x_{min}))$ in the x direction in the step 1.
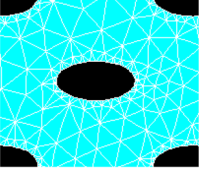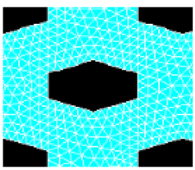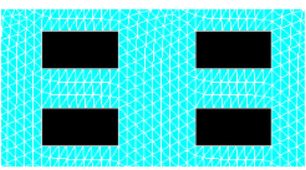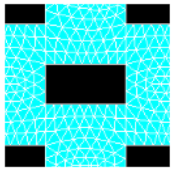
(2) Load case 2:

    (a) DOF constraints are removed from the extreme right and a uniform compression is applied to the extreme top.

    (b) Step (1b) is repeated for E_{yy}^{eff} and ν_{yx}^{eff}.

Four different pore geometries have been considered namely elliptical, hexagonal, rectangular with uniform alignment and alternating pattern. With $\alpha = 1$ the pore shapes transform into circles or uniform polygons. Images shown in Table 1 represent a part of the geometry.

Seven different aspect ratios have been considered for each pore shape with pore alignment in Configuration 1, i.e., α from 0.1 to 1.0. Configuration 2 for each of the above aspect ratios was modeled by substituting $\alpha_2 = 1/\alpha_1$, where the subscripts represent the configuration number. Thus, a total of thirteen cases were considered with α from 0.1 to 10.0.

As the aspect ratio approaches values much higher or lower than unity, the radius of curvature drastically reduces at the tip of the ellipse. To capture the effect of stress concentration, additional mesh refinement is performed at the critical locations. For polygon shaped pores such mesh refinement is performed close to the vertices of the pore.

Table 1 Variation of pore shape

Elliptical/circular	Hexagonal	Rectangular	
		Aligned	Alternating

Five different levels of porosity, p from 0.05 to 0.5, were considered here for each pore shape and aspect ratio. The pore size is given by the effective radius $r_{eff} = \sqrt{\frac{A}{\pi}}$, and the size of the structure is given by the average side length l of the planar geometry. Pore sizes with $\frac{r_{eff}}{l}$ value from 0.01 to 0.1 in fifty uniform steps were considered in this study.

Results and Discussion

Benchmarking of the Numerical Technique

Although the scope of this work is to study the effects of pores of uniform size and distribution on the stiffness of the porous structure, the numerical analysis seeks a benchmark against the theoretical and empirical relations discussed in the introduction.

Thus, for the benchmarking of the numerical method, square (1 mm × 1 mm) planar (plane stress with unit thickness) geometries, with random circular pores, net porosity ranging from 2.5 to 30%, were analyzed. The pore radius randomly varies from 0.01 to 0.03 mm and pore locations are also random yet obeying a proximity criterion (minimum gap of 0.01 mm) from the boundaries and the neighboring pores to avoid conjoined pores and meshing difficulties. The random pore sizes and locations are generated using a MATLAB script and an APDL script is used to generate the solid model and to perform the rest of the analysis. The structures were loaded along the x axis and the effective Young's modulus was found by dividing the reaction forces at the boundary by the side length of the square geometry.

For a high value of net porosity, the program would keep on generating random pore sizes and locations but it would fail the proximity criterion. To make the process more efficient the operation is done in two steps. In the first step, the program would generate the random pore sizes and sort them in the descending order. In the second stage the random locations are generated for the biggest pore size to the smallest pore size. However, using random pore size and distribution a maximum net porosity slightly more than 30% could be achieved.

Figure 8a–c shows the pore distribution with random pores for three different levels of porosity. Figure 8d shows the variation of normalized stiffness (Young's modulus) with net porosity. The final output to this analysis is the stiffness vs. porosity plot which shows an exponential fit (Eq. 18), similar to the expression (Eq. 2) presented by Duckworth [2] and Spriggs [3].

$$\frac{E}{E_0} \approx \exp(-bp) \tag{18}$$

While Spriggs [3] listed b values ranging from 1.6 to 4.35, here b is found to be 2.632. Thus, the value seems to be reasonably close.
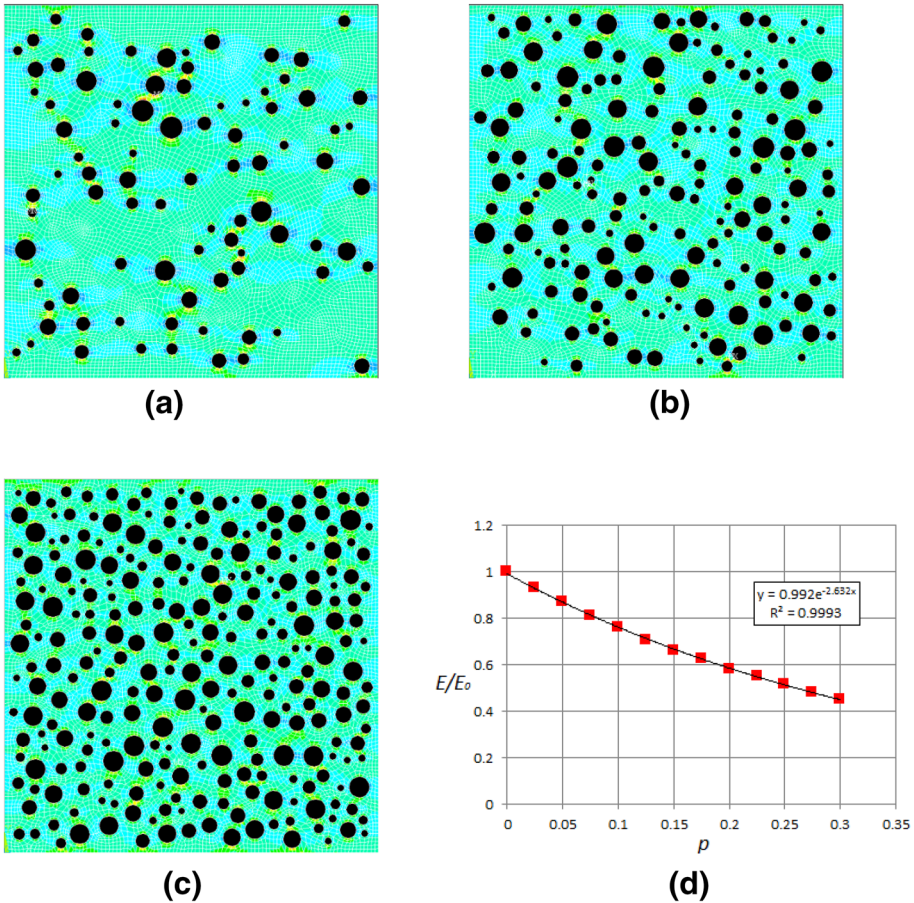
Fig. 8 Porous structures with random circular pores for different porosities and effect of porosity on stiffness. **a** 10% porosity. **b** 20% porosity. **c** 30% porosity. **d** FE results versus exponential fit

Variation of Young's Moduli with Net Porosity and Aspect Ratio

The following figures show the variation of Young's moduli with net porosity at various aspect ratios for elliptical pores. Figure 9a shows the variation of E_{xx} with porosity and Fig. 9c shows the variation of E_{yy} with porosity. For the clarity of visualization only three aspect ratios, i.e., $\alpha = 0.1, \alpha = 1.0, \alpha = 10.0$ are shown here. The curves for intermediate aspect ratios lie in between these curves. The plots shown with circular and square dots (markers) are the results of ANSYS simulations whereas the continuous lines represent the best empirical fit for such variation. The empirical relation has the following form.

$$\frac{E}{E_0} = 1 - c_0 \times p^{c_1}, \tag{19}$$

where, c_0, c_1 are dependent on the aspect ratio α. Thus, the critical porosity at which the stiffness of the material becomes zero is given by $p_{cr} = \left(\frac{1}{c_0}\right)^{\frac{1}{c_1}}$. Same expression (Eq. 19)
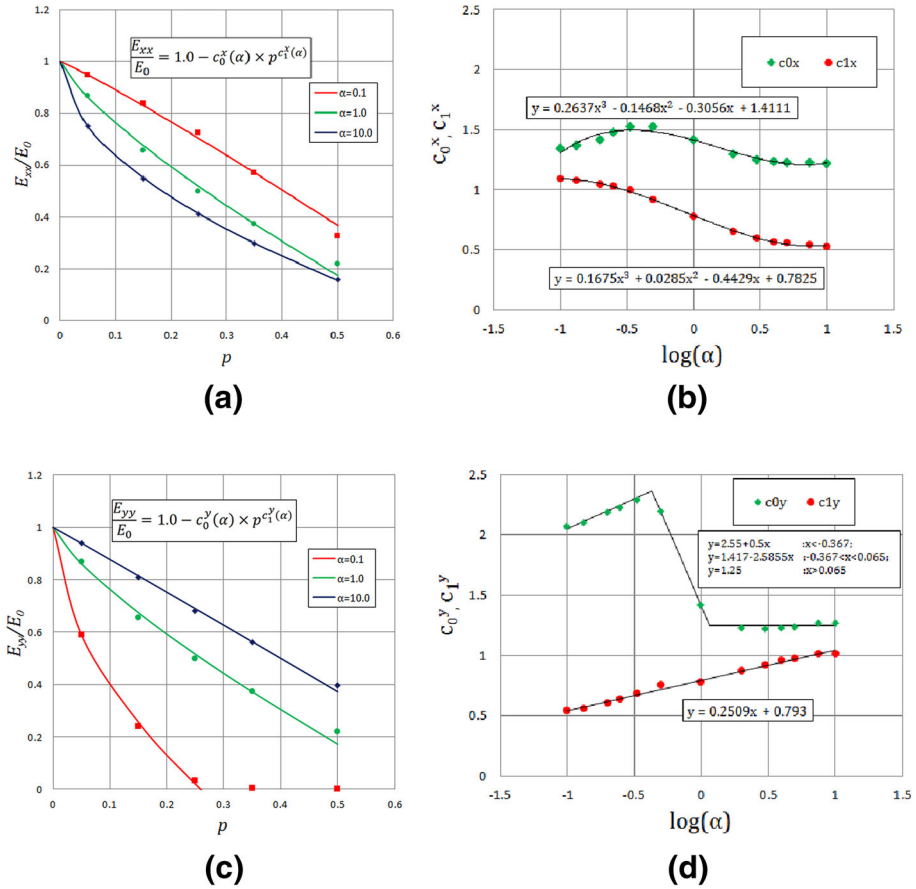
Fig. 9 Variation of normalized Young's moduli with porosity for elliptical pores. **a** E_{xx} versus p. **b** c_0^x, c_1^x versus aspect ratio. **c** E_{yy} versus p. **d** c_0^y, c_1^y versus aspect ratio

can be used to represent the variation of Young's modulus in either x or y direction; however, the coefficients c_0 and c_1 are different for different directions.

The first thing which is noticed is that the two Young's moduli are different. This does not agree with most literature presenting empirical, semi-empirical or fully theoretical formulae. In those classical works however the pores are considered circular (spherical in 3-D) and not elliptical and the essence of an aspect ratio is brought into only to consider the variation of pore size in the third dimension, thus facilitating pore types from needle shape to disk shape.

Thus, the coefficients c_0, c_1 are different in x and y directions. Superscript x or y is used to denote the coefficients in a given direction. The variations of c_0^x, c_1^x with respect to α are shown in the Fig. 9b. The empirical fits for the variations are given by the following equations.

$$c_0^x = 0.2637\chi^3 - 0.1468\chi^3 - 0.3056\chi + 1.4111 \tag{20}$$
$$c_1^x = 0.1675\chi^3 + 0.0285\chi^2 - 0.4429\chi + 0.7825, \tag{21}$$
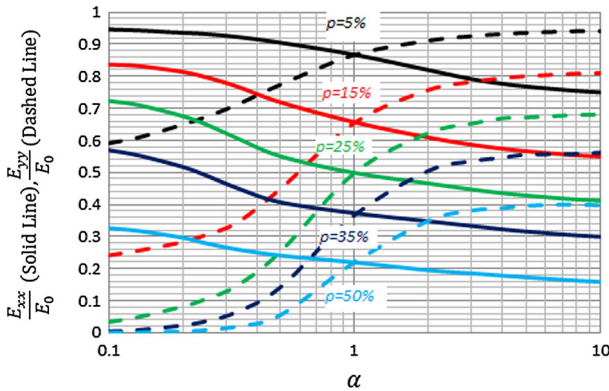
where, $\chi := \log_{10}\alpha$.

Fig. 10 Variation of normalized Young's moduli with aspect ratio for elliptical pores

The variations of c_0^y, c_1^y with respect to α are shown in Fig. 9d. The empirical fits for such variations are given by the following equations.

$$c_0^y = 2.55 + 0.5\chi \quad if \quad \chi \leq 0.367$$
$$= 1.417 - 2.5855\chi \quad if \quad 0.367 < \chi \leq 0.065$$
$$= 1.25 \quad if \, \chi > 0.065 \tag{22}$$
$$c_1^y = 0.2509\chi + 0.793 \tag{23}$$

Figure 10 on the other hand shows the variation of E_{xx} and E_{yy} with α for various percentage of porosity. The plot is semi-logarithmic in x, to provide equal emphasis on $\alpha < 1$ and $\alpha > 1$. It is seen that with aspect ratio changing gradually from 0.1 to 10, E_{xx} monotonically decreases and E_{yy} monotonically increases for all levels of porosity.

From Fig. 9 it can be seen that not only is $E_{xx}(p,\alpha) \neq E_{yy}(p,\alpha)$, but also $E_{xx}(p,\alpha) \neq E_{yy}(p,\frac{1}{\alpha})$ and vice-versa. This is also evident from the asymmetry of the plots in the Fig. 10. From the "Geometry and Meshing" $E_{yy}^1(p,\frac{1}{\alpha}) := E_{xx}^2(p,\alpha)$ and $E_{xx}^1(p,\frac{1}{\alpha}) := E_{yy}^2(p,\alpha)$. Thus, $E_{xx}^1(p,\alpha) \neq E_{xx}^2(p,\alpha)$ and $E_{yy}^1(p,\alpha) \neq E_{yy}^2(p,\alpha)$. Therefore, with the same value of porosity and the same size, shape and aspect ratio the Young's moduli may differ substantially only because of the change in relative orientations of the neighboring pores. The exception to this behavior is at $\alpha = 1$, i.e., for circular pores. Then, $E_{xx}^2(p,1) := E_{yy}^1(p,1) = E_{xx}^1(p,1) := E_{yy}^2(p,1)$.

When α is less than unity then E_{yy} is less than E_{xx}. The situation reverses when $\alpha > 1$. When $\alpha = 1$, the two Young's moduli have the same value. This observation remains true throughout the range of porosity. This may be attributed to the stress concentration at the sharp tips of the major axes.

Variation of Young's Moduli with Pore Size

The variation of the Young's moduli with pore size for circular pores with 25% porosity has been presented here. For uniformly distributed circular pores, E_{xx} and E_{yy} are expected to be same. However, the two values showed slight difference which seems to increase with the pore size (Fig. 11). When the pore size is about 10% of the whole geometry, i.e., $\frac{r_{eff}}{l} \approx 0.1$, such difference is about $0.15 E_0$. With increasing pore size, it is not necessarily true that $E_{xx} > E_{yy}$ or vice-versa and the variation is random. However, that the range of variation
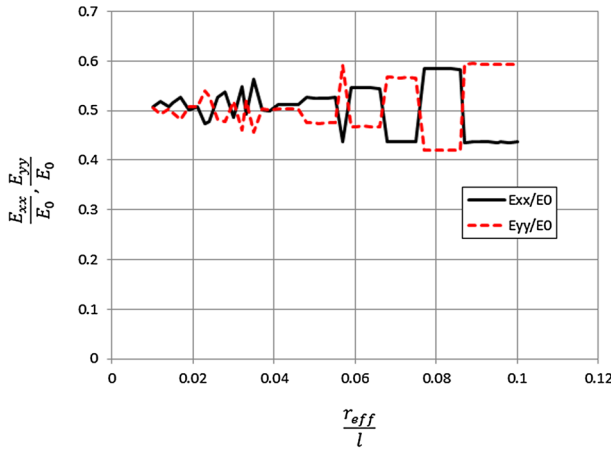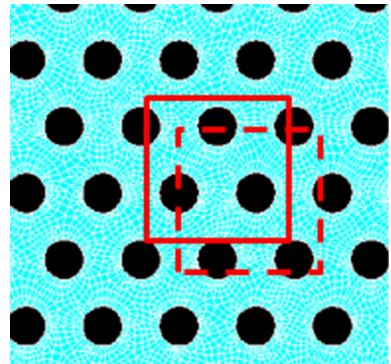
Fig. 11 Effect of pore size on Young's Moduli for circular pores

Fig. 12 Pore selection: localization effect. *Note*: Both squares encompass equal porosity but have different pore distributions
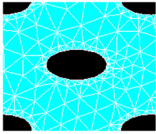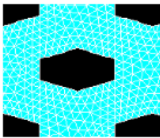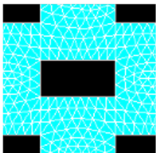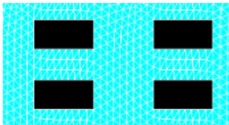

increases with $\frac{r_{eff}}{l}$ while the average of the two moduli i.e. $\frac{E_{xx}+E_{yy}}{2}$ remains approximately constant over the range of pore size.

With $p = 0.25$ for circular pores this average value is $\approx 0.5E_0$ which is also the same for randomly oriented pores as could be verified from Fig. 8d. Similar observation is made for all other porosity levels. Therefore it can concluded that for circular pores ($\alpha = 1$), the stiffness of the structure is solely dependent on the net porosity and Eq. (18) holds true irrespective of the size of the pores and whether the pores are randomly or systematically arranged.

A possible explanation could be that with smaller pore size, the pore distribution approaches uniformity and tend to behave like a homogenous material and the material loses its homogeneity as the pore size increases. If the specimen size were also increased by the same factor as the pore size, no such behavior would be observed since, $\frac{r_{eff}}{l}$ remains a constant. However, if the specimen size does not change, the situation would be equivalent to enclosing and inspecting a smaller region from a uniform distribution of pores. Depending on the boundary (shown with solid and broken lines in Fig. 12) chosen, the local level stiffness would be different and slightly off from the uniform global value.

Table 2 Variation of Young's moduli with pore shape

	$p = 0.05$		$p = 0.15$		$p = 0.25$		$p = 0.35$		$p = 0.50$	
	$\frac{E_{xx}}{E_0}$	$\frac{E_{yy}}{E_0}$	$\frac{E_{xx}}{E_0}$	$\frac{E_{yy}}{E_0}$	$\frac{E_{xx}}{E_0}$	$\frac{E_{yy}}{E_0}$	$\frac{E_{xx}}{E_0}$	$\frac{E_{yy}}{E_0}$	$\frac{E_{xx}}{E_0}$	$\frac{E_{yy}}{E_0}$
$\alpha = 0.1$	0.95	0.59	0.84	0.24	0.72	0.03	0.57	4e − 3	0.33	5e − 4
$\alpha = 1$	0.87	0.87	0.66	0.65	0.50	0.50	0.37	0.37	0.22	0.22
$\alpha = 10$	0.75	0.94	0.55	0.81	0.41	0.68	0.30	0.56	0.16	0.40
$\alpha = 0.1$	0.95	0.60	0.84	0.27	0.72	0.05	0.60	5e − 3	0.37	4e − 4
$\alpha = 1$	0.86	0.86	0.64	0.64	0.48	0.48	0.35	0.35	0.19	0.18
$\alpha = 10$	0.73	0.95	0.51	0.81	0.36	0.68	0.23	0.56	0.08	0.40
$\alpha = 0.1$	0.95	0.61	0.83	0.27	0.70	0.05	0.56	4e − 3	0.38	3e − 4
$\alpha = 1$	0.87	0.87	0.67	0.65	0.54	0.58	0.44	0.36	0.31	0.19
$\alpha = 10$	0.79	0.94	0.62	0.79	0.51	0.65	0.41	0.52	0.30	0.36
$\alpha = 0.1$	0.94	0.79	0.79	0.62	0.65	0.51	0.52	0.41	0.36	0.30
$\alpha = 1$	0.87	0.87	0.68	0.68	0.54	0.54	0.44	0.44	0.31	0.31
$\alpha = 10$	0.79	0.94	0.62	0.79	0.51	0.65	0.41	0.52	0.30	0.36

Variation of Young's Moduli with Pore Shape

It was found that in association to aspect ratio and pore size, pore shape plays a significant role in deciding the stiffness of the porous structure. The findings are summarized in the Table 2.

Following observations are made from this table:

A. For a given value of porosity and aspect ratio, the values of Young's moduli may vary slightly or substantially with pore shape depending on the net porosity. For smaller values of porosity the variation is small and the variation increases with increase in porosity. For instance with $p = 0.05$ and $\alpha = 10$, the ratio $\frac{E_{xx}}{E_0}$ lies between 0.73 and 0.79 and $\frac{E_{yy}}{E_0}$ lies between 0.94 and 0.95. However, for $p = 0.5$ and $\alpha = 10$), $\frac{E_{xx}}{E_0}$ lies between 0.08 and 0.30 and $\frac{E_{yy}}{E_0}$ lies between 0.36 and 0.40.

B. Over the range of p, for a given aspect ratio, E_{yy} seems to have less variation with pore shape than E_{xx}.

C. For elliptical, hexagonal and aligned rectangular pore shapes, at all levels of porosity, with $\alpha = 1$, values of the E_{xx} and E_{yy} are same. This however, is not true for rectangular alternating pores.

D. At all levels of porosity the aligned and alternating rectangular pattern behave closely when it comes to E_{xx}. However, when it comes to variation of Young's modulus in y
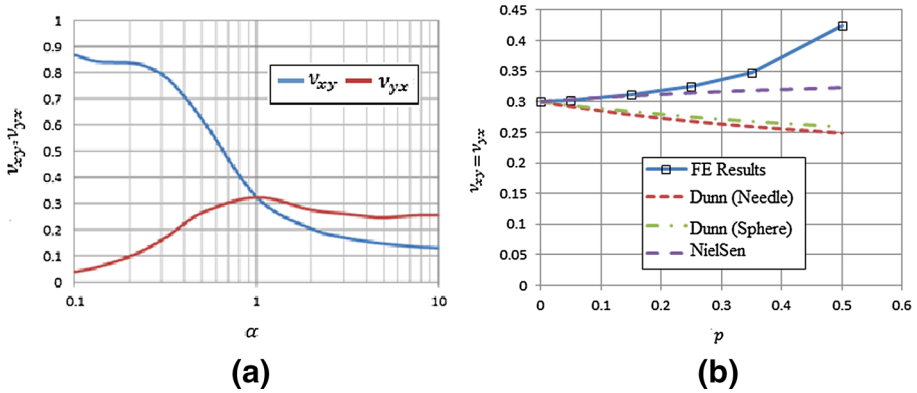
Fig. 13 Variation of Poisson's ratios with aspect ratio and porosity. **a** Poisson's ratios versus α for $p = 0.25$. **b** Poisson's ratio versus p for $\alpha = 1$

directions, alternating rectangular pores find more similarity with elliptical or hexagonal pores than the aligned rectangular pores.

E. Finally, with upto 35% porosity, results of elliptical pores effectively represent the behavior of hexagonal and rectangular alternating pores for all aspect ratios.

Variation of Poisson's Ratios with Porosity and Aspect Ratio

Figure 13a, b shows the variation of Poisson's ratios with aspect ratio respectively. For the variation of ν_{xy} and ν_{yx} with aspect ratio, only $p = 0.25$ is presented here. At all other levels of porosity the variation remains similar yet the orders of magnitude are different. Also, only the cases of elliptical pores have been presented here. For other type of pores, similar variations of Poisson's ratios are observed.

It is already seen that at lower aspect ratios the material is stiffer in x direction than in y direction and the situation reverses in the higher range of aspect ratios. The same observation is repeated with these plots. When $\alpha < 1$, the porous structure more easily contracts/expands in y direction when elongated/compressed in x direction than its contraction/expansion in x direction when elongated/compressed in y direction. Thus, $\nu_{xy} > \nu_{yx}$. The situation reverses when $\alpha > 1$. The two Poisson's ratios are same at $\alpha = 1$. The two Poisson's ratios differ in values and in some cases go much higher or lower than the nominal Poisson's ratio, i.e., of the original material. However, the equality of the expressions $\frac{\nu_{xy}}{E_{xx}}$ and $\frac{\nu_{yx}}{E_{yy}}$ is observed to remain true. This can be confirmed from Fig. 14. Thus, the bulk behavior of the porous structure can be modeled as a linear elastic orthotropic material.

To show the variation of Poisson's ratios with the amount of porosity (Fig. 13b), the case of circular pores have been presented here. Since with circular pores $\nu_{xy} = \nu_{yx}$, one needs to show only one variable. As could be seen from Fig. 13b, none of the classical expressions matches with the FE results. The expression based on Nielsen's formula however shows some agreement upto $p = 0.3$. As $p \to 0$, the Poisson's ratio approaches the nominal value, i.e., 0.3, of the original material. As the porosity increases, Poisson's ratio also increases. If the Poisson's ratio in z direction were to be the same, one would expect the isotropic Poisson's ratio would settle before the theoretical limit 0.5. However, no such settling trend is observed in the given range of porosity. At $p = 0.5$, Poisson's ratio $\nu_{xy} = \nu_{yx} \approx 0.425$. Thus, it can be said in the given range of porosity, structure becomes more and more incompressible with increasing p. The term incompressibility is relative here. It does not indicate an extremely
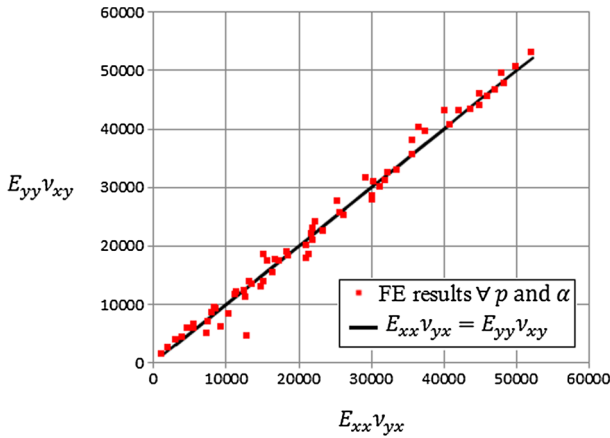
Fig. 14 Consistency of Poisson's ratios in relation to orthotropic behavior

large value of the bulk modulus rather it refers to a substantially higher stiffness in volumetric deformation compared to the stiffness in longitudinal deformation.

Variation of Shear Modulus with p and α

For the completion of the discussion on an orthotropic material, the variation of shear modulus must also be kept in focus. Figure 15 presents the variation of G_{xy} with aspect ratio for different levels of porosity. The aspect ratio $\alpha > 1$ simply refers to Configuration 2. Thus,

$$G_{xy}^1 \left(p, \frac{1}{\alpha} \right) = G_{xy}^2 (p, \alpha) \tag{24}$$

Unlike the moduli of elasticity the shear modulus does not show a monotonically increasing or decreasing variation. For a given level of porosity it starts from a small value for $\alpha \ll 1$, attains a maximum value between $\alpha = 0.5$ and $\alpha = 1$ and then again starts decreasing to a smaller value as $\alpha \gg 1$.

The maximum value however remains smaller than the nominal value, $G_0 = \frac{E_0}{2(1+\nu_0)}$.

For a given value of porosity, shear modulus varies with aspect ratio in an asymmetric bell-shaped curve (Fig. 15) with the maximum value at an aspect ratio below unity. The behavior may be explained from Fig. 16 which show shear deformation of square plates with single elliptical pores. The diagrams are however only schematic and does not represent actual deformations.

If the aspect ratio is inverted, i.e., $\alpha_2 = \frac{1}{\alpha_1}$, where α_1, α_2 are the aspect ratios of the pores in the Fig. 15a, b respectively, then only the sense of x and y directions are interchanged. Thus, with the shown deformation both the cases would yield the same G_{xy}. Therefore, a plot of G_{xy} versus α would be symmetric about $\alpha = 1$. However, the structures considered here have many pores and setting $\alpha_2 = \frac{1}{\alpha_1}$ will not only switch the sense of directions but the relative pore orientation will also change from Configuration 1 to Configuration 2 as shown in Fig. 5. Thus, the curves are not symmetric about $\alpha = 1$. However, with $\alpha = 1$, the porous structure behaves as an isotropic material in the $x - y$ plane. The relation of isotropy given by Eq. (25) can be confirmed from Fig. 17.
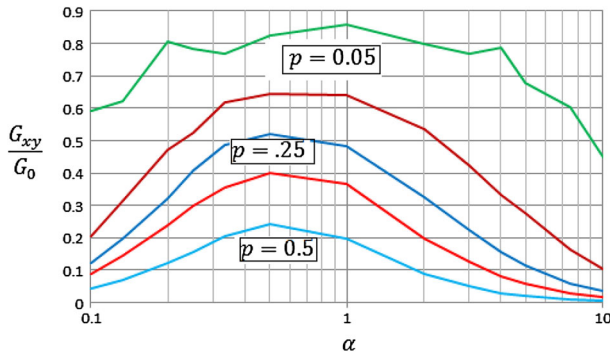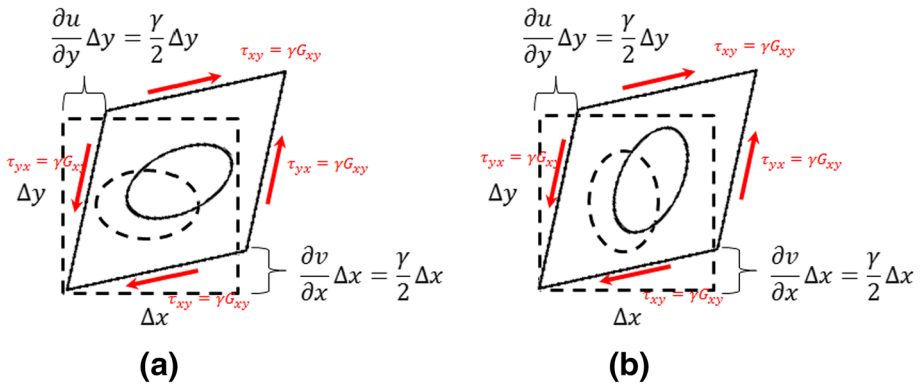
Fig. 15 Variation of G_{xy} with p and α

Fig. 16 Shear deformation of single elliptical pore. **a** $\alpha_1 < 1$. **b** $\alpha_2 = \frac{1}{\alpha_1} > 1$
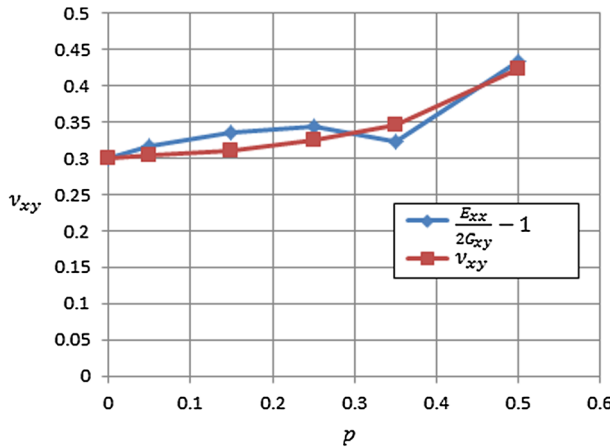

Fig. 17 Correlation among Young's modulus, shear modulus and Poisson's ratio ($\alpha = 1$)

$$v_{xy} = \frac{E_{xx}}{2G_{xy}} - 1 = \frac{(1 + v_0)\, E_{xx}/E_0}{G_{xy}/G_0} - 1 \tag{25}$$

The minor difference is due to the fact that, E_{xx}/E_0 and G_{xy}/G_0 are very close and when substituted into the above equation yields numerical errors.

Conclusions

The study presented above shows in detail the variation of the elastic properties of a porous materials with the net porosity and different pore attributes such as aspect ratio, orientation etc.

For circular pores, it is shown that the correlation between Young's modulus and the net porosity approximately follows the same exponentially decaying curve irrespective of the pore distribution being random or systematic. This developed equation closely resembles the relationship proposed by Duckworth [2] and Spriggs [3]. This behavior was isotropic due to the nature of the pores.

For systematically oriented pores the behavior was not isotropic. However a single general equation (Eq. 19) is proposed to describe the effect of net porosity p and aspect ratio α on Young's moduli E_{xx} and E_{yy} although with different set of coefficients.

In reference to the variation of the elastic moduli, pore shape proved to be less critical than pore aspect ratio. Also, the pore size did not significantly change the "average" value of the Young's modulus yet a higher pore size meant higher variation about the average value. It can be attributed to the position of the pores. The variation of shear modulus and Poisson's ratio clearly show that the material behavior is orthotropic.

Compliance with ethical standards

Conflict of interest The authors declare that they have no conflict of interest.

References

1. Dewey, J.M.: The elastic constants of materials loaded with nonrigid fillers. J. Appl. Phys. **18**, 578–581 (1947). doi:10.1063/1.1697691
2. Duckworth, W.H.: Precise tensile properties of ceramic bodies. J. Am. Ceram. Soc. **34**, 1–9 (1951)
3. Spriggs, R.M.: Expression for effect of porosity on elastic modulus of polycrystalline refractory materials, particularly aluminium oxide. J. Am. Ceram. Soc. **44**, 628–629 (1961)
4. Wang, J.C.: Young's modulus of porous materials. J. Mater. Sci. **19**, 801–808 (1984)
5. Phani, K.K., Niyogi, S.K.: Young's modulus of porous brittle solids. J. Mater. Sci. **22**, 257–263 (1987)
6. Ramakrishnan, N., Arunachalam, V.S.: Effective elastic moduli of porous solids. J. Mater. Sci. **25**, 3930–3937 (1990)
7. Tatsuhiko, A., Sakka, S.: Dependence of elastic moduli of porous silica gel prepared by sol–gel method on heat-treatment. J. Mater. Sci. **25**, 4732–4737 (1990)
8. Choren, J.A., Heinrich, S.M., Silver-Thorn, M.B.: Young's modulus and volume porosity relationships for additive manufacturing applications. J. Mater. Sci. **48**, 5103–5112 (2013). doi:10.1007/s10853-013-7237-5
9. Dunn Martin, L., Ledbetter, H.: Poisson's ratio of porous and microcracked solids: theory and application to oxide superconductors. J. Mater. Res. **10**, 2715–2722 (1995). doi:10.1557/JMR.1995.2715
10. Nielsen, L.F.: Elastic properties of two-phase materials. Mater. Sci. Eng. **52**, 39–62 (1982)
11. Daniel, A., Haber, R.A., Watchman, J.B.: Elastic properties of porous silica derived from colloidal gels. J. Am. Ceram. Soc. **73**, 3376–3381 (1990)
12. Phani, K.K., Dipayan, S.: Critical reevaluation of the prediction of effective Poisson's ratio for porous materials. J. Mater. Sci. **40**, 5685–5690 (2005)
13. Nielsen, L.F.: Elasticity and damping of porous materials and impregnated materials. J. Am. Ceram. Soc. **67**(2), 93–98 (1984)

14. Phani, K.K., Dipayan, S.: The relations between the shear modulus, the bulk modulus and Young's modulus for porous isotropic ceramic materials. Mater. Sci. Eng. A **490**, 305–312 (2008). doi:10.1016/j.msea.2008.01.030
15. Mori, T., Tanaka, K.: Average stress in matrix and average elastic energy of materials with misfitting inclusions. Acta Metall. **21**, 571–574 (1973)
16. Meguid, S.A., Cheon, S.S., El-Abbasi, N.: FE modelling of deformation localization in metallic foams. Finite Elem. Anal. Des. **38**, 631–643 (2002)
17. De Girogi, M., et al.: Aluminium foams structural modelling. Comput. Struct. **88**, 25–35 (2010)
18. Badiche, X., et al.: Mechanical properties and non-homogeneous deformation of open-cell nickel foams: application of the mechanics of cellular solids and of porous materials. Mater. Sci. Eng. A **289**, 276–288 (2000). doi:10.1016/j.compstruc.2009.06.005
19. Sid-Ali, K., et al.: Finite element simulation of mechanical behaviour of nickel-based metallic foam structures. J. Alloys Compd. **471**, 147–152 (2009). doi:10.1016/j.jallcom.2008.03.069
20. Kovacik, J.: Correlation between Young's modulus and porosity in porous materials. J. Mater. Sci. **18**, 1007–1010 (1999)
21. https://in.pinterest.com/pin/141863456984208861/
22. https://www.flickr.com/photos/alan_cressler/2134762319/in/faves-jrosenk/
23. https://www.google.com/patents/US20130017759/
24. http://www.gla.ac.uk/ibls/US/fab/tutorial/generic/bone2.html
25. Bin, D., Min, W.: Customized Ca-P/PHBV nanocomposite scaffolds for bone tissue engineering: design, fabrication, surface modification and sustained release of growth factor.J. R. Soc. Interface **7**, S615–S629 (2010). doi:10.1098/rsif.2010.0127.focus
26. Lawrence, M., et al.: Next generation orthopaedic implants by additive manufacturing using electron beam melting. Int. J. Biomater. (2012). doi:10.1155/2012/245727